2010 IEEE International Conference on Robotics and Automation
Anchorage Convention District
May 3-8, 2010, Anchorage, Alaska, USA

Design and Development of a 3-Axis MRI-compatible Force Sensor

U-Xuan Tan[1], Bo Yang[1], Rao Gullapalli[2], and Jaydev P. Desai[1], *Senior Member, IEEE*
[1]*Robotics, Automation, Manipulation, and Sensing (RAMS) Laboratory*
Department of Mechanical Engineering, University of Maryland, College Park, MD, USA
[2]*University of Maryland School of Medicine, Baltimore, MD, USA*
Email: uxtan@umd.edu, yangbo@umd.edu, rgullapalli@umm.edu, jaydev@umd.edu

Abstract— **Magnetic resonance imaging (MRI) has been gaining popularity over standard imaging modalities like ultrasound and CT because of its ability to provide excellent soft-tissue contrast. However, due to the working principle of MRI, a number of conventional force sensors are not compatible. One popular solution is to develop a fiber-optic force sensor. However, the measurements along the principal axes of a number of these force sensors are highly cross-coupled. One of the objectives of this paper is to minimize this coupling effect. In addition, this paper describes the design of an elastic frame structure that is obtained systematically by an algorithm and not purely based on design intuition. We used a topology optimization technique, which has two major advantages: 1) aids engineers in design when given a constrained boundary, and 2) optimize the displacement amplification, which will in turn increase stiffness, bandwidth, and improve sensing resolution. To ensure that the frames are linked from the input to output, a solution for topology optimization is proposed. The sensor is then fabricated using plastic material (ABS) as it is one of the ideal material for MRI environment. However, the hysteresis effect seen in the displacement-load graph of plastic materials is known to affect the accuracy. Hence, this paper also proposes modeling and addressing this hysteretic effect using Prandtl-Ishlinskii play operators. Finally, experiments are conducted to evaluate the sensor's performance, as well as its compatibility in MRI under continuous imaging.**

I. INTRODUCTION

In recent years, a number of groups have used magnetic resonance imaging (MRI) because MRI provides excellent soft-tissue contrast. In addition, MRI does not emit harmful ionizing radiation. Unfortunately, due to its working principle, MRI environment poses many challenges. The components required to obtain a good MR image consist of: 1) strong magnetic fields (1.5T or 3T), 2) spatial and temporal field gradients, 3) radio frequency pulses, and 4) sensitive signal coils used for detection [1]. Any device developed for use in MRI needs to be appropriately designed to maintain excellent image quality. Ferro-based metals are not permitted because of the strong magnetic field. Non-ferro-based metals which can conduct electricity are used with caution as eddy currents can be generated due to the strong switching magnetic field gradients.

One of the key devices of a robotic system is the force sensor, which can be used for control purposes, and haptic feedback so that surgeons have a better "feel" when teleloperating the slave robot in the MRI bore. Researchers have proposed a couple of MRI-safe force sensors. One of the commercially available force sensors is a piezoresistive based sensor. The sensor is classified as MRI safe because no force is generated on the sensor. However, the sensor produces a localized artifact [1]. This affects the image and hence cannot be placed next to the target location.

Researchers have also proposed using optical methods [2]–[7]. Hirose and Yoneda [2] were one of the pioneers in developing fiber-optic force sensor. Tada *et al*. [3] modified the sensor to make it usable in MRI environment, while Takahashi *et al*. [4] proposed a 6-axis fiber-optic force sensor. Tada and Kanade [5] and Tokuno [6] proposed using lens to improve the sensing performance. Recently, Puangmali *et al*. [7] proposed using a pair of bent-tip optical fibers to detect the displacement. Most of these flexure-based designs are sensitive to moments. In addition, the measurement along the axes of most of these multi-axes sensors are highly coupled and accuracy is affected when forces/moments from different axes are applied. The angle between the emitter/reflector and the receiver is dependent on the forces and moments in all the axes. Hence, this paper presents a simple design of decoupling the measurements.

An elastic frame structure is also required for these force sensors. Most present designs of the elastic frame structure are based on intuition. Hence, a topology optimization algorithm is used to generate a suitable design for the sensor. The primary goal of using topology optimization algorithm in our prototype is to derive a systematic analytical process to design the fiber-optic based force sensor for increased stiffness, bandwidth and sensing resolution. In a number of cases, the algorithm outputs a design with very thin thickness, which are challenging to fabricate. Hence, a solution is also proposed in this paper for the topology optimization to ensure continuity between the input and output of the design.

Plastic material is commonly used in the elastic frame structure for MRI-compatibility. However, most plastic materials exhibit hysteretic force-displacement relationship due to the strain energy absorbed during deformation. Hence, the play operator of Prandtl-Ishlinskii is proposed to model this hysteretic effect to improve the sensing accuracy.

In section II, we present the sensor design with its sensing principle. Next, the design of the elastic frame structure using topology optimization is presented in section III and section IV presents the prototype developed. Section V discusses the calibration, which includes accounting for the hysteretic

We would like to acknowledge the support of NIH grant 1R01EB008713.

effect. Section VI covers the experimental results and section VII concludes the paper.

II. SENSOR

Fig. 1 provides an overview of a typical fiber-optic force sensor. The light source emits light via the optical cable to the force sensor. At the same time, there is an optical cable at the receiving end to transmit the light back into the control room, where all the non-MRI compatible equipment is stored. The photo sensor, located in the control room, senses the light intensity and the opto-electronic circuitry converts the intensity into appropriate voltage signal. Electrical wires, which act as antennas and pick up RF signals and corrupt the image quality, are thus eliminated in MRI room.

The fundamental principle to obtain the displacement on the elastic frame structure is by measuring the change in light intensity. There are five general sensing principles to obtain the displacement as summarized by Hirose and Yoneda [2]. The underlying sensing principle that is adopted in this paper is the reflective intensity method proposed by Puangmali *et al*. [7], [8]. This section introduces the adopted sensing principle, followed by the design of the sensor.

A. Sensing Principle

The sensing principle used in our prototype is the reflective intensity principle, which is illustrated at the bottom of Fig. 1. There is a pair of optical fiber cables with their tip rigidly placed at an angle, α, and a distance, a, apart. The core diameter of the optical cable is d. A reflector, on an elastic frame structure, is placed at a distance, h, away from the optical cables. A force on the loading point will cause a deformation in the elastic frame structure, resulting in a displacement in the reflector a change in the intensity of the reflected light. Hence, by monitoring the reflected light intensity, the force can be computed.

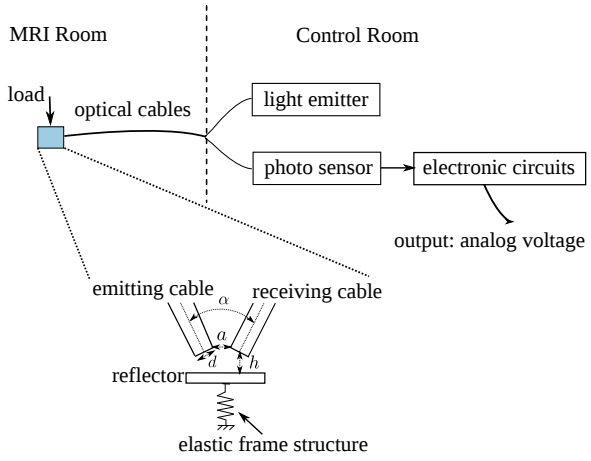

Fig. 1. Overview of a typical MRI-compatible fiber-optic force sensor

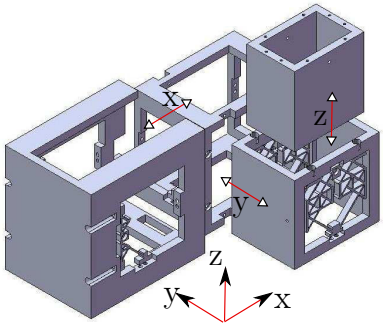

Fig. 2. Design of the force sensor

The parameters shown in Fig. 1, especially the angle between the two cables α, are factors that affect the sensing fidelity. An in-depth analysis of this sensing technique has been presented by Puangmali *et al*. [7], [8].

B. Sensor Design

The intended application of this sensor is for a manipulator designed for radiofrequency ablation of tumors under continuous MRI [9]. The desired design specifications are:

- Measurement axes are decoupled as much as possible,
- Maximize input-output displacement amplification,
- Include a through space at the center for instruments like a needle driver, and
- Attach all the cables onto the same sensor's face to lower the chances of the cables being entangled.

To ensure that the force measurements along the three principal directions are decoupled, it is important to design the sensor geometry that will enable motion along the principal direction of application of force while ensuring that no motion takes places in the other two principal directions. Fig. 2 shows the design of our sensor. It consists of 3 prismatic joints placed along 3 independent axes in series. Two elastic frame structures are attached to each prismatic joint. The purpose of these elastic frame structures are: 1) to provide the spring stiffness, 2) to provide an input-output displacement gain, and 3) to change the direction of displacement to allow all the fiber-optical cables to be connected from the bottom (see design specification above). The design of these elastic frame structures is a challenging task for engineers and it is desired that a systemic algorithm can be used and written as a program to aid engineers. Hence, a topology optimization method is presented in the next section.

III. DESIGN OF ELASTIC FRAME STRUCTURE USING TOPOLOGY OPTIMIZATION

A normal process of developing the elastic frame structure usually starts with the designing of the mechanism, followed by simulations using methods like finite element analysis (FEA) before building the prototype. The initial design phase is often the most challenging and depends greatly on experience and creativity. In this paper, a topology optimization technique for compliant mechanisms based on the methodology in [10] is used to present a systematic way of designing the required mechanisms.

A. Topology Optimization

Topology optimization of compliant mechanisms has been developing in the past 15 years [10]–[14]. A comparative study of the various methods and problems has been presented by Deepak *et al*. [12].

The resolution of the force sensor is dependent on the output displacement. Given a fixed range of input load to be sensed, the resolution of the force sensor improves as the range of output displacement increases. In addition, it is desired that the stiffness experienced by the input is high, since a high stiffness will result in smaller displacement on the input, and also larger bandwidth. The topology optimization method proposed by Saxena and Ananthasuresh [10] fits the requirements and is hence adopted in this paper.

A continuum can be approximated using finite element method and the element used in this paper is frames (which are similar to beams, except that axial loads and axial deformations are included) with design variables, x, as the out-of-plane width of each frame. In this paper, x, are initialized to be 2 mm.

First, consider an arbitrary design domain with known loading and boundary conditions as illustrated in Fig. 3(a), where F_{in} is the input force, and Δ_{out} is the output displacement. The method used to solve this problem is unit dummy load method. Hence, the discretized displacement field, $\mathbf{U}$, due to the input force, F_{in}, is given by:

$$\mathbf{F} = \mathbf{KU} \tag{1}$$

where $\mathbf{F}$ is the input force vector, and $\mathbf{K}$ is the structure stiffness matrix. Similarly, the displacement field, $\mathbf{V}$, due to the unit dummy load can be obtained using:

$$\mathbf{F}_{\text{d}} = \mathbf{KV} \tag{2}$$

where $\mathbf{F}_{\text{d}}$ is the dummy load force vector. The mutual potential energy, MPE, and the output displacement, Δ_{out}, is given by:

$$\Delta_{\text{out}} = MPE = \mathbf{V}^T\mathbf{KU} \tag{3}$$

The output displacement and mutual potential energy has the same numerical value because unit dummy load is used. The strain energy stored can also be computed as:

$$SE = \frac{1}{2}\mathbf{U}^T\mathbf{KU} \tag{4}$$

The objective function proposed by Frecker *et al*. [15] is used in this paper to maximize the ratio of output and input displacement and is given by:

$$\Phi = -\frac{MPE}{SE} \tag{5}$$

A design is obtained by minimizing the objective function.

B. Ensuring linkage between input and output

Due to the limitation of manufacturing technology, there is a minimum required thickness of the frame elements. In a number of cases, the optimization algorithm tends to produce a design that has very thin frame elements which ultimately breaks the continuity between input and output. Furthermore, some of these extremely thin frame elements are also not practically realizable due to machining constraints.

Approaches like filtered distortion energy approach and restrained local, relative rotation approach [11] have been proposed to obtain a distributed compliant mechanisms for 4 nodes quad elements. In this paper, frames are used and the two-above mentioned approaches cannot be applied directly. Hence, a solution to this problem is proposed in paper.

The general idea of the proposed method is to ensure that there are 0, 2, or more frames (large enough for fabrication) at the more critical nodes. In this paper, the more crucial nodes are chosen to be the nodes with the 8 frames connecting to it. A filter function to differentiate frames that meet the required minimum width, is proposed as:

$$f(x_j) = \frac{\frac{\pi}{2} + \tan^{-1}\left(P\left(x_j - C\right)\right)}{\pi} \tag{6}$$

where x_j is the width, P is an arbitrary large number (10^{12}), and C (2.5mm) is the minimum thickness needed. This filter function will output a value of 0 for frames whose width is smaller than C and 1 for width greater than C. Any frame's thickness that is less than 2.5mm is treated as non-existent during the fabrication of the elastic frame structure.

Next, the following constraint is imposed in the optimization algorithm for all the critical nodes:

$$-\left(\sum_{j=1}^{8}\left(f(x_j)\right) - 1\right)^2 + c_0 \leq 0 \tag{7}$$

where c_0 is set to 0.5. It is not advisable to choose all the nodes as critical nodes as this will significantly increase the number of constraints, in turn affecting the optimization result. Hence, only nodes with 8 frames are chosen as the critical nodes. The purpose of these constraints is to greatly penalize when only 1 frame is attached to the critical node.

In this force sensor, two types of mechanism are required. Fig. 3(a) shows the boundary condition for the first mechanism. It is desired that the vertical input force creates a displacement in the vertical direction. To reduce the number of design variables, symmetry is used and is shown in Fig. 3(a). Using Matlab to solve the optimization problem, the output design is shown in Fig. 3(b) based on topology optimization. With regards to the second mechanism, it is desired to use the horizontal input force to realize a vertical displacement. Using symmetry, Fig. 4(a) shows the boundary and loading conditions and Fig. 4(b) shows the design output from topology optimization. Although the reflector will rotate when loaded, the amount of rotation will be small. In addition, this rotation is only dependent on the load along that principal axis.

IV. PROTOTYPE

To save cost and allow complexity in the design, a flexure-based frame structure is built using a rapid prototyping (RP) machine. A fused deposition modeling (FDM) machine, which is classified as solid-based [16], is used to build the prototype. The heated head deposits plastic (ABS for this prototype) in a paste-like form. RP machines can build complicated designs which may be difficult or impossible to realize by conventional machining techniques. In addition, plastic is the preferred material for MRI and it is a challenge to fabricate thin plastic flexure joints using conventional

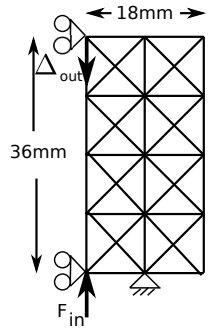

(a) Boundary and loading conditions for the first mechanism

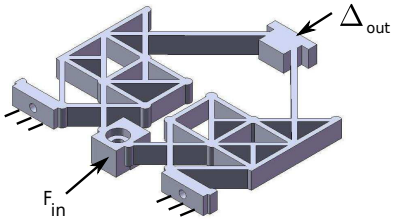

(b) Mechanism realized from topology optimization algorithm for conditions shown in Fig. 3(a)

Fig. 3. Boundary conditions and results for the first mechanism

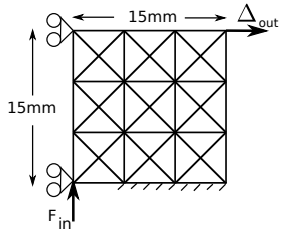

(a) Boundary and loading conditions for the second mechanism

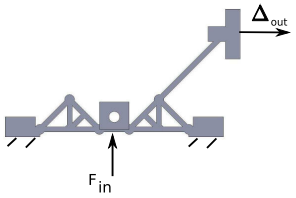

(b) Mechanism realized from topology optimization algorithm for conditions shown in Fig. 4(a)

Fig. 4. Boundary conditions and results for the second mechanism

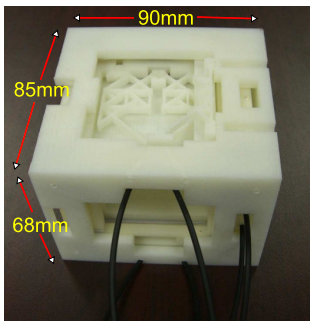

Fig. 5. Prototype of the 3-DOF MRI compatible force sensor

machining. Finally, Rapid prototyping machines enable us to build the parts rapidly and ready for use in 1-2 days.

The optical fiber cable selected in this prototype is Keyence FU-77, which has a core diameter of 1.13mm, because of its large diameter and bending flexibility. The photosensor in our prototype is from Keyence and the model is FS-V31M. Fig. 5 shows a photo of the prototype fiber-optic based MRI compatible 3-DOF force sensor.

V. CALIBRATION

When a force is exerted on the force sensor, the matrix, **A**, is multiplied to the force to obtain the individual forces imparted onto the individual elastic frame structure. Each of these forces is then passed through the individual structure's hysteretic effect (Ω) to obtain the voltage as illustrated in Fig. 6. To estimate the load from voltage measurements, the voltage measurements are first passed through the inverse

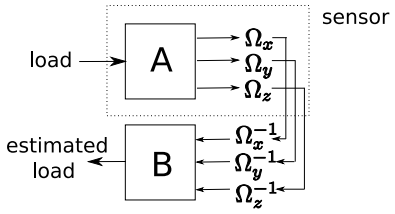

Fig. 6. Estimation of external load through sensors' output

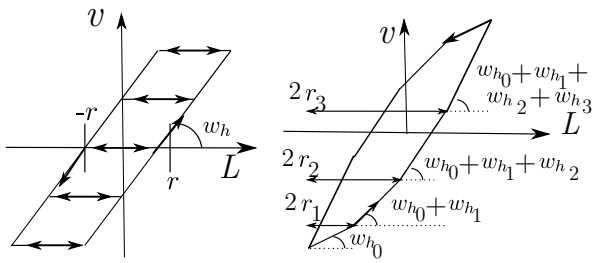

(a) Play operator

(b) Summing up 4 play operators with different threshold values

Fig. 7. Prandtl-Ishlinskii hysteresis model

hysteretic model of each individual elastic frame structure. The output vector is then pre-multiplied by **B**, which is ideally the inverse of **A**, to obtain the applied load information.

A. Modeling of the hysteretic effect

Plastic materials, while ideal for MRI imaging, are known for their hysteretic force-deformation characteristic. It is proposed in this paper that the Prandtl-Ishlinskii (PI) operator be used to model this hysteretic effect. The PI operator has been commonly used in controlling hysteretic plants and an in depth explanation is available in [17], [18].

Play Operators

The play operator in the PI hysteresis model, commonly used to model the backlash between gears, is defined by:

$$\begin{aligned} v_i(t) &= H_r[L_i, v_{i_0}](t) \\ &= max\{L_i(t) - r, min[L_i(t) + r, v_i(t-T)]\} \end{aligned} \quad (8)$$

where L is the input load to the elastic frame structure, v is the voltage reading from photosensor, r is the threshold value or the magnitude of the backlash, T is the sampling period and i represents the respective elastic frame structure. Fig. 7(a) illustrates how the play operator behaves. The initial Condition of (8) is given by:

$$v_i(0) = max\{L_i(0) - r, min[L_i(0) + r, v_{i_0}]\} \quad (9)$$

where v_{i_0} is a real number which is usually initialized to 0. To change the gradient, a weight value w_h is multiplied to the play operator H_r . By summing a number of such operators with different threshold values and weights, a hysteresis model is obtained:

$$v_i(t) = \vec{w}_h^T \vec{H}_r[L_i, \vec{v}_{i_0}](t) \quad (10)$$

where $\vec{w}_h^T = [w_{h_0} ... w_{h_n}]$ is the weight vector, $\vec{H}_r[L_i(t), \vec{v}_{i_0}] = [H_{r_0}\left[L_i(t), v_{i_{0_0}}\right] \dots H_{r_n}\left[L_i(t), v_{i_{0_n}}\right]]^T$,

threshold vector $\vec{r} = [r_0 \dots r_n]^T$ (where $r_n > \dots > r_0, r_0 = 0$), and the initial state vector is $\vec{v}_{i_0} = [v_{i_{0_0}} \dots v_{i_{0_n}}]^T$. Fig. 7(b) shows the effect when 4 play operators with different threshold values are summed up.

Inverse Parameters

The inverse PI model is commonly expressed using the stop operators. Kuhnen [17] showed that the inverse PI model can be expressed by PI play operators too. Thus, the inverse of the PI model can also be expressed as:

$$\begin{aligned} \hat{L}_i(t) &= \Omega_i^{-1}[v_i(t)] \\ &= \vec{w}_{h'}^T \vec{H}_{r'} \left[v_i(t), \vec{L}'_{i0} \right](t) \end{aligned} \tag{11}$$

The inverse model parameters can be calculated by:

$$w'_{h_0} = \frac{1}{w_{h_0}}; w'_{h_i} = \frac{-w_{hi}}{\left(\sum_{j=0}^{i} w_{h_j}\right)\left(\sum_{j=0}^{i-1} w_{h_j}\right)}, i = 1 \dots n;$$

$$r'_i = \sum_{j=0}^{i} w_{h_j} (r_i - r_j); y'_{0_i} = \sum_{j=0}^{i} w_{h_j} y_{0_i} + \sum_{j=i+1}^{n} w_{h_j} y_{0_j};$$

$$r_0 = 0; i = 0 \dots n; \tag{12}$$

B. Calibration Matrix

Two sets (training and testing) of data were obtained. Applying least squares errors to the training set, we obtained:

$$\mathbf{B} = \begin{pmatrix} 0.9593 & 0.0789 & 0.0693 \\ -0.1787 & 0.9854 & -0.1123 \\ 0.1557 & -0.1662 & 0.9972 \end{pmatrix} \tag{13}$$

where **B** is ideally the inverse of **A**. Since the diagonal values of **B** are significantly larger than the off-diagonal terms in the matrix, it indicates a relatively strong decoupled effect in our 3-axis force sensor prototype.

VI. EXPERIMENTS

Experiments were conducted to evaluate the performance of the force sensor and also to check its MRI compatibility.

A. Experimental Results

A force sensor (MDB-2.5 by Transducer Techniques) was used to apply a force in the three principal directions, namely x-, y- and z- axis. Two sets of experiments were conducted, with the first being the training set for calibration and the second set for evaluation. Fig. 8 shows the result from the testing set of the voltage output from the photosensors. The dashed line in Fig. 8 is the model obtained from the training set discussed in section V(A), and it can be seen that the test data fits the model well. This indicates that the data obtained is repeatable and that the hysteresis model can be used.

Fig. 9 shows the final result of the estimated force from the force sensor versus actual loading on the force sensor. The main factor that is limiting the performance of this prototype is friction. Friction is the contributing factor for the very gentle gradient after primary turning point and its inverse is a very steep gradient, thus making the sensor's output sensitive to noise. The dotted lines in Fig. 9 represents the range of friction, which is approximately 1N. It can be seen that most of the errors are within this range and the performance of the sensor can be improved significantly if friction is minimized in our design. Table I summarizes the result.

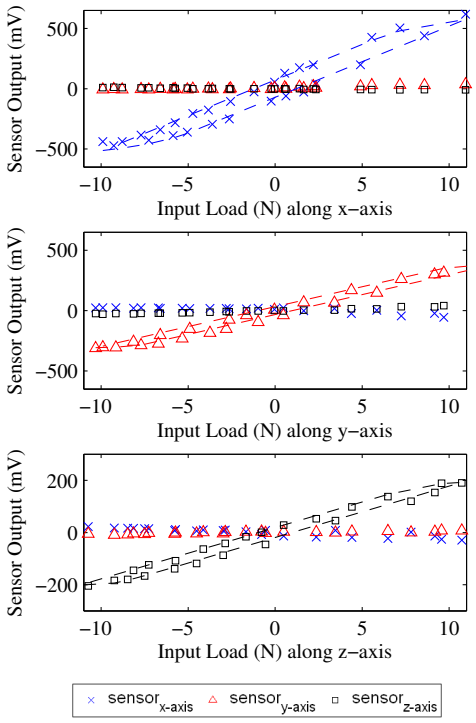

Fig. 8. These three graphs show the output voltage of the test set from the photosensors against load applied along the three principal axis respectively. The dash line in each graph is the hysteresis model obtained from the training set described in section V(A).

TABLE I
EXPERIMENTAL RESULTS

direction of loading	$x_{RMS\text{-}error}$	$y_{RMS\text{-}error}$	$z_{RMS\text{-}error}$
x-axis	0.469	0.476	0.664
y-axis	0.557	0.686	0.782
z-axis	0.295	0.233	0.486

This table summarizes the RMS errors of the sensor when a force is applied along the three principal axes. All the readings are in N.

B. Magnetic Resonance Imaging

Images of the force sensor are also taken using the MRI machine to illustrate that no artifacts are formed in the images. The force sensor is placed inside a cylinder filled with water to provide the contrast for imaging. Fig. 10(a) shows one of the images taken. A phase mapping that is sensitive to magnetic field in-homogeneity is also taken and is shown in Fig. 10(b). The white portion area in Fig. 10(a) indicates water. Clear edges of the force sensor can be seen and this shows that no artifacts were present. Furthermore, minimum phase differences are seen in the phase mapping image (Fig. 10(b)) which shows that little or negligible magnetic field distortion is created by the force sensor. Hence, the use of this sensor in the MRI will not affect the image quality of the soft-tissue being imaged.

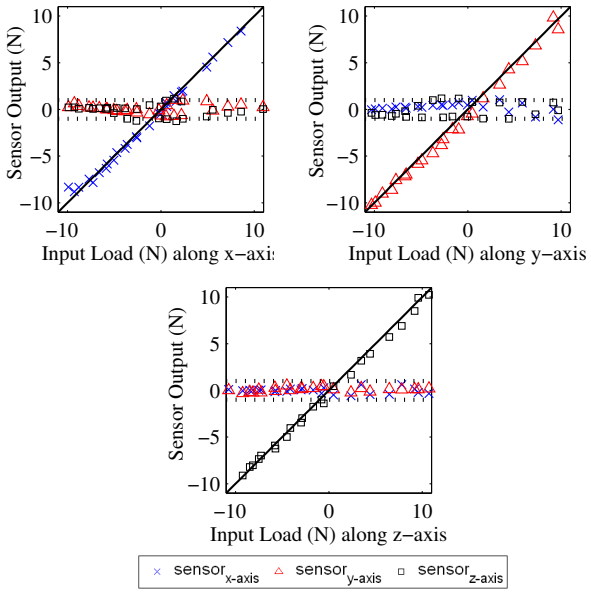

Fig. 9. This figure shows the sensor output vs input load along the 3 principal axis. The dotted lines indicate the range of friction, which is approximately 1N. The sensor performance is linear along the principal directions as expected from analysis.

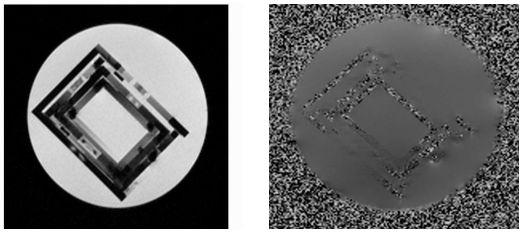

(a) Image of the force sensor under MRI

(b) Phase mapping image of the force sensor in MRI

Fig. 10. MRI compatibility test

VII. CONCLUSION & DISCUSSION

This paper presents an fiber-optic force sensor that can be used in MRI under continuous imaging. There are generally two main phases in developing a usable fiber-optic force sensor, namely: 1) design of the elastic frame structure, and 2) calibration to estimate the load from the photosensors' voltage measurements. This paper has presented a systematic way of using a topology optimization algorithm to design the elastic frame structure, and in the process, a solution to ensure physical linkage between the input and output of the mechanism obtained from the algorithm is proposed. A calibration method using Prandtl-Ishlinskii is also proposed to account for the hysteretic behavior. A prototype of the force sensor was developed and evaluated.

Friction is determined to be the limiting factor in the performance of this prototype. The authors plan to reduce the friction by fabricating the prismatic joints using better material and machining techniques. One possibility would be to use non-ferrous metals with rounded edges and fabricate the sensor using electrical discharge machining (EDM). This will enable a more compact footprint as well as reduced (or potentially negligible) hysteretic effect.

ACKNOWLEDGMENTS

The authors would like to thank Prof Linda C. Schmidt of University of Maryland for the usage of her rapid prototyping machine.

REFERENCES

[1] H. Elhawary, Z. T. H. Tse, A. Hamed, M. Rea, B. L. Davies, and M. U. Lamperth, "The case for MR-compatible robotics: a review of the state of the art," *International Journal of Medical Robotics and Computer Assisted Surgery*, vol. 4, pp. 105–113, March 2008.

[2] S. Hirose and K. Yoneda, "Development of Optical 6-Axial Force Sensor and its Signal Calibration Considering Non-Linear Interference," in *Proc. IEEE International Conference on Robotics and Automation*, Cincinnati, OH, USA, May 1990, pp. 46–53.

[3] M. Tada, S. Sasaki, and T. Ogasawara, "Development of an Optical 2-axis Force Sensor Usable in MRI Environments," in *Proc. IEEE Sensors*, Orlando, Florida, USA, June 2002, pp. 984–989.

[4] N. Takahashi, M. Tada, J. Ueda, Y. Matsumoto, and T. Ogasawara, "An Optical 6-axis Force Sensor for Brain Function Analysis using fMRI," in *Proc. IEEE Sensors*, Toronto, Canada, Oct. 2003, pp. 253–258.

[5] M. Tada and T. Kanade, "An MR-Compatible Optical Force Sensor for Human Function Modeling," in *Proc. of the international Conference on Medical Image Computing and Computer Assisted Intervention*, 2004, pp. 129–136.

[6] T. Tokuno, M. Tada, and K. Umeda, "High-Precision MRI-Compatible Force Sensor with Parallel Plate Structure," in *Proc. of the International Conference on Biomedical Robotics and Biomechatronics*, Scottsdale, AZ, USA, Oct. 2008, pp. 33–38.

[7] P. Puangmali, K. Althoefer, and L. D. Seneviratne, "Novel Design of a 3-Axis Optical Fiber Force Sensor for Applications in Magnetic Resonance Environments," in *Proc. IEEE International Conference on Robotics and Automation)*, Kobe, Japan, May 2009, pp. 3682–3687.

[8] P. Puangmali, H. Liu, K. Althoefer, and L. D. Seneviratne, "Optical Fiber Sensor for Soft Tissue Investigation during Minimally Invasive Surgery," in *Proc. IEEE International Conference on Robotics and Automation)*, Pasadena, CA, USA, May 2008, pp. 2934–2939.

[9] R. Kokes, K. Lister, R. Gullapalli, B. Zhang, A. MacMillan, H. Richard, and J. P. Desai, "Towards a teleoperated needle driver robot with haptic feedback for RFA of breast tumors under continuous MRI," *Medical Image Analysis*, vol. 13, no. 3, pp. 445–455, June 2009.

[10] A. Saxena and G. K. Ananthasuresh, "On an optimal property of compliant topologies," *Structural and Multidisciplinary Optimization*, vol. 19, no. 1, pp. 36–49, March 2000.

[11] L. Yin and G. K. Ananthasuresh, "Design of Distributed Compliant Mechanisms," *Mechanics Based Design of Structures and Machines*, vol. 31, no. 2, pp. 151–179, 2003.

[12] S. R. Deepak, M. Dinesh, D. K. Sahu, and G. K. Ananthasuresh, "A Comparative Study of the Formulations and Benchmark Problems for the Topology Optimization of Compliant Mechanisms," *Journal of Mechanisms and Robotics*, vol. 1, no. 1, p. 011003, Feb. 2009.

[13] O. Sigmund, "On the design of compliant mechanisms using topology optimization," *Mechanics of structures and machines*, vol. 25, no. 4, pp. 493–524, 1997.

[14] O.Sigmund, "Morphology-based black and white filters for topology optimization," *Structural and Multidisciplinary Optimization*, vol. 33, pp. 401–424, 2007.

[15] M. I. Frecker, G. K. Ananthasuresh, N. Nishiwaki, N. Kikuchi, and S. Kota, "Topological synthesis of compliant mechanisms using multicriteria optimization," *ASME Journal of Mechanical Design*, vol. 119, no. 2, pp. 238–245, 1997.

[16] C. K. Chua, K. F. Leong, and C. S. Lim, *Rapid Prototyping: Principles and Applications in Manufacturing (2nd edition)*. World Scientific Publishing Company Inc., 2003.

[17] K. Kuhnen, "Modeling, Identification and Compensation of Complex Hysteretic Nonlinearities: A modified Prandtl-Ishlinskii Approach," *European Journal of Control*, vol. 9, no. 4, pp. 407–418, 2003.

[18] W. T. Ang, C. N. Riviere, and P. K. Khosla, "Feedforward controller with inverse rate-dependent model for piezoelectric actuators in trajectory tracking applications," *IEEE/ASME Trans. Mechatronics*, vol. 12, no. 2, pp. 1–8, Apr. 2007.